International Journal of Advanced Research in Engineering and Technology (IJARET)
Volume 11, Issue 3, March 2020, pp. 224-239, Article ID: IJARET_11_03_020
Available online at http://www.iaeme.com/IJARET/issues.asp?JType=IJARET&VType=11&IType=3
Journal Impact Factor (2020): 10.9475 (Calculated by GISI) www.jifactor.com
ISSN Print: 0976-6480 and ISSN Online: 0976-6499

EXPERIMENTAL INVESTIGATION ON BEACH MORPHODYNAMICAL PROCESS NEAR RIVER MOUTH

S. Di Ronza, Di Natale M., C. Eramo, V. Minutolo*, S. Palladino, R. Zona

SFS DEMON LAB, Engineering Department, University of Campania "L.Vanvitelli", Via Roma 29 - 81031, Aversa (CE), Italy

*Corresponding Author E mail: vincenzo.minutolo@unicampania.it

ABSTRACT

Physical model study on wave influences on river-mouth depositional process is presented. Experiments were performed in a wave basin in order to determine erosion and accretion area due to the combined wave – current flows. An inflow glass channel was designed to reproduce a river mouth model in a 3D wave basin made with a sand bottom. The tests were carried out under three different conditions: river current, waves, wave –current interaction. Measurements of wave heights, beach profiles and bathymetric profiles were made. The results show that in the presence of combined wave-current flows, erosion areas are more evident in vicinity of a mouth with depth and width values greater than depth and width values of inflow channel.

Keywords: physical model, wave –current interaction, beach profiles and bathymetric profiles, erosion areas

Cite this Article: S. Di Ronza, Di Natale M., C. Eramo, V. Minutolo*, S. Palladino, R. Zona, Experimental Investigation on Beach Morphodynamical Process Near River Mouth, *International Journal of Advanced Research in Engineering and Technology (IJARET),* 11 (3), 2020, pp 224-239.
http://www.iaeme.com/IJARET/issues.asp?JType=IJARET&VType=11&IType=3

1. INTRODUCTION

Wave-current interaction may significantly influence coastal circulation and sediment transport. This interaction typically occurs at estuaries, where waves propagate opposite to the to the river flow direction. This wave–current interaction may affect both the downstream river reach and the near shore zone close to the estuary, potentially resulting in important morphodynamical changes with complex erosion or depositional patterns. The strongly non-linear coupling of the current-wave motion and the induced morphological changes adds up to the complexity in the study of these phenomena.

Several numerical and experimental models have been developed with the aim of describing the hydrodynamics of wave-current interaction [1,2,3,4,5]. The author [1] obtained a theoretical expression for the variation of the momentum spreading rate of surface jets due to the action of opposite surface gravity waves. The theory predicts a linear increase in the spreading rate of the jet, within the established flow zone. Koole and Swan [3] carried out a novel experimental investigation in which compared the jet spreading in presence of waves to that in a fluid at rest. This comparison highlights the additional wave-induced mixing and shows that the oscillatory wave motion has a significant effect upon both the mean velocity profiles and the magnitude of the turbulent fluctuations. Di Natale et al. [5] experimentally investigated the velocity distribution in a heated water discharge issuing from a rectangular channel at the tank water surface (warm water discharged from a rectangular channel at the free surface of the reservoir). The results provided a procedure to evaluate the variation of the velocity field due to the wave – jet velocity based on the relevant dimensionless parameters. Morphological changes induced by wave and current have also been experimentally studied. Skafel [6] related measured velocity field and erosion rate in the nearshore zone. The measurements have con-firmed the rules of wave orbital bottom velocity and turbulent jets in the erosion of cohesive shores. The author demonstrated the link between plunging breaking and high erosion rates. Movable-bed model experiments were run to define an equilibrium area for different tidal periods and sediments [7]. The authors investigated the relationship among channel area, tidal period, tidal prism, and maximum channel velocity. Experimental data may help define the tidal prism-minimum channel cross-sectional area relationship in the midrange channel size. An experimental investigation of erosion profile (storm profile) was carried out in a wave flume using regular waves [8]. As a result, an equation was proposed providing a better fit of the experimental data fitted compared to the previously developed equation. Experiments carried out within the SANDS project are presented by Caceres et al. [9]. This project includes the bottom evolution experiments done at three different flumes (Hannover, Barcelona and Delft) operating at three different scales (prototype, 1:2 and 1:6 respectively), and the development and performance assessment of a novel measurement equipment. The obtained results of "identical" experiments performed at the three flumes show that a scaling of 1:2 leads to bottom evolution results almost identical to prototype under erosive conditions. However, for smaller scales, there is transport in a larger area outside the foreshore slope and thus larger morphodynamical differences appear with respect to the prototype. The results obtained under accretive wave conditions show bigger differences between the three scaled flumes and a limited capacity to promote shoreline accretion. Lee et al. [10] analysed the hydrodynamic characteristics of a river mouth by performing hydraulic experiments to investigate wave-current interaction by building a river mouth model in a 3-D wave basin. Using the results of these hydraulic experiments, the Authors analysed the hydrodynamic characteristics of the region in which wave-current coexist in the river channel and in the vicinity of the river mouth. They observed that, in a river channel, the turbulence flow field develops more rapidly when both waves and current are present as opposed, compared with a situation where no current exists and the changes in the wave heights, bot-tom flow, and horizontal velocity distributions in the areas where wave-current coexist in the river mouth. The measured horizontal velocity distribution shows the influence of the flow field on the combined effects of the wave and current velocity components. Finally, the Authors detected a close relationship between the wave-current interaction and the sediment transport near the river mouth. With a view to developing a morphodynamical model able to be applied to coastal areas like river mouths and lagoons, a finite volume 2DH morphodynamical model is implemented, which can consider the effect of the regular wave field in both hydrodynamics and morphodynamics [11]. Moreover, secondary flow effects on bed load are also considered. The model is based on an accurate shock-capturing and C-property preserving scheme, also able to describe shock phenomena properly [12]. The model is suited for the study of complex 2D domains, with a minimum number of physically based parameters to be considered in sediment transport problems. A few different theories have been implemented and applied to some benchmark tests, in order to carry out a comparison between them. A trench migration test was conducted with and without a regular wave, propagating in the same direction of the current. The model's results show a better agreement with experimental data using a non-equilibrium approach for the suspended load. Pascolo et al. [13] investigated the effects induced by bottom shear stress on the spectral propagation of the waves against the jet current. The model used is based on classic shallow-water equation on the wave action balance and it was applied to literature test. The comparison shows that the present model provided a very adequate representation of the hydrodynamics of a turbulent jet confined to the bottom. In this paper the study of coastal morphodynamical processes close to a river mouth was carried out in the 3D wave basin of the Hydraulics Laboratory of the University of Campania "L. Vanvitelli". In the experimental installation, it was possible to simulate the morphological processes by a current discharged in a wave tank with a sandy bottom. The aim of the experimentation was to highlight coastal morphodynamical processes in vicinity of the river mouth due first to the action of: (i) the current without waves, (ii) the waves without current and (iii) combined wave-current flow. The results showed that combined wave-current flows determine more evident erosion areas in vicinity of river mouth compared with the conditions without interaction. Furthermore, it was possible to identify and assess the effects due to wave-current interaction introducing dimensionless relevant parameters as in case of coupled sub-marine pipelines in the launch phase, where the phenomena are hardly governed by current-wave flows too [20].

2. EXPERIMENTAL SETUP

The experimental equipment (Figure 1) is composed of the following parts:

- wave basin and wave generating system
- hydraulic circuit for simulation of river mouth
- measurement equipment

2.1. Wave Basin and Wave Generating System

The wave basin is 15.70 m wide and 12.45 m long. The operating water depth, h, ranges from 040m to 0.60m. The fixed concrete bed slope is 1:20 for a 10 m length. The bottom material in the basin is formed by well-sorted sand with D50 = 0.20 mm and rs = 2600 kg/m3 (Figure 1). A wave-generator with a non-reflective generation system is used to produce right angle and oblique incident waves using a snake-front piston-type paddle system that has 30 wave-paddles and actuators. Wave absorbers are used to reduce the waves reflected from the side and rear walls of the wave basin. A wave-absorbing beach is used to reduce the wave energy on the shore side. The wave generation software used for controlling the paddle system is AWASYS, developed by Coastal Engineering Laboratory of University of Aalborg. The absorbing wave system [14] is operated by non-recursive linear digital filters working in real time [15,16,17].

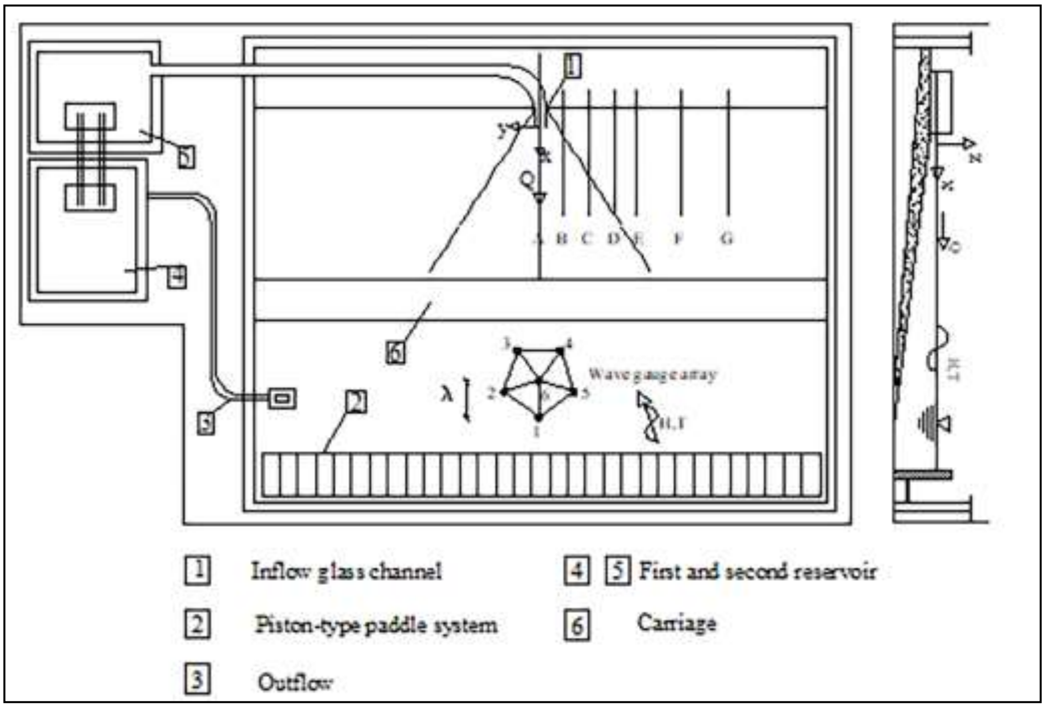

Figure 1 Scheme of the experimental installation- Measurement mesh.

2.2. Hydraulic Circuit for River Mouth Simulation

The inflow glass channel (Figure 1 (1)) for river mouth simulation is located inside the 3D-wave basin. The first reservoir (Figure 1 (5)), 2.40 m long, 1.80 m wide, and 2.80 m deep is connected to the wave basin by inflow glass channel. The channel is made of plexiglass and is 10.00 m long, 0.30 m height and 0.40 m wide. The outflow (Figure 1 (3)), located below the floor level at 2 m from the wave paddle is connected with the second reservoir (Figure 1 (4)), 2.40 m long, 1.20 m wide, and 2.80 m deep, connected by two vertical centrifugal pumps (Q = 2 ÷ 60 l/s) to the first reservoir in all the experimental runs. The channel slope is i = 0.0005.

2.3. Measurement Instrumentation

Wave heights are measured by 30 resistance probes with a sampling rate of 20 Hz. Measurements of beach profiles and bathymetric profiles are made with a Conventional Profiler M5 L Laser setting on the carriage (Figure 1 [6]). Flow field measurements are carried out by an ultrasonic Doppler velocimeter with a sampling frequency equal to 20 Hz.

2.4. Experimental Test

The tests carried out at the Hydraulics Laboratory were performed by submitting sand bottom material to the following conditions:

- current alone
- wave alone
- combined wave –current flows

We conducted experiments on the wave-current interaction near the river mouth for 26 cases (Table 1). The case studies were created by varying the wave heights (H=3÷7 cm), wave periods (T = 0.67 ÷ 1 s), wave propagation angles (dd = 0 and dd = 20°), and discharge flow rates of the river (Q = 0.002 ÷ 0.005 m3/s). The incident waves were established by calibrating the wave paddle before installing the river mouth model, while the incidence discharge flow was adjusted by installing the river mouth model and regulating the valve of the pumps (Figure 1). The hydraulic conditions at the channel outflow have been determined from the steady flow profile for each given discharge (Q = 0.002 ÷ 0.005 m3/s). Flow profile resulted to be an accelerated one in a mild-slope channel with critical depth, hc, occurring at the river mouth.

Regular waves were calibrated for two different wave directions. Figure 2 shows a wave spectrum for H = 0.07 m, T = 1 s and dd = 20°.

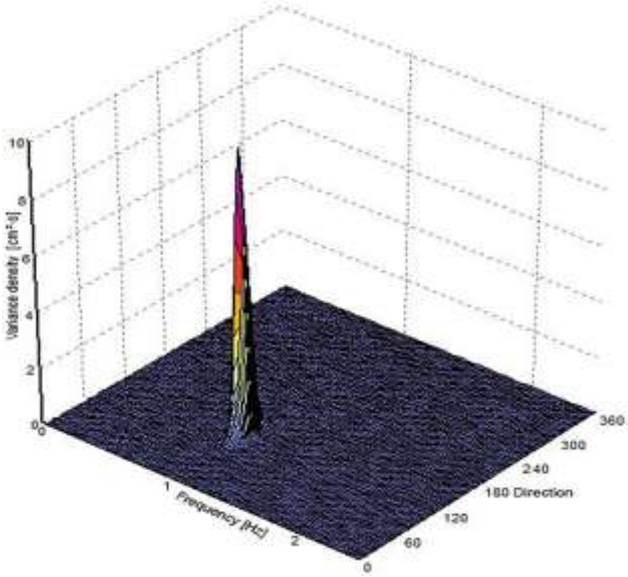

Figure 2. Example of wave spectra measured.

The length and celerity of the waves are estimated based on the first – order Stokes wave theory. The water level was measured using six resistance probes located on wave gauges array (Figure 1). In order to enable the estimation of the directional spectrum of the incident wave field, the probes were installed on array with a distance λ equal to 0.25 L [18]. The array was located at distance to 3.20 m from the wave paddles at the water depth 0.40 m. All these measurements were made at 20 Hz frequency. In all the experimental runs with combined wave-current flows, the waves were generated after the pumps were activated and steady flow condition was attained. In addition, all the measurements were carried out after the transient of the wave-current region. Furthermore, the wave - current interaction (test 9 ÷ 26) was performed after generating first a flow rate Q = 0.002 m3/s and then a wave with H = 0.03 m, T = 0.67 s dd = 0° on the sand bottom material with i0 = 0.05 (initial profile). It was assumed that the beach profile reached after the action of Q = 0.002 m3/s and H = 0.03 m, T = 0.67 s dd = 0° is the initial modelling profile. This condition represents what happens in coastal processes when a full flow and a storm could occur after low flows in a very flat sea surface that took place during prolonged dry weather, or after small sea waves without any outflow.

The water depth, hv, was 0.58 m deep and kept constant for all the tests.

Table 1. Incident wave and current condition used for hydraulic model tests.

Test	H (m)	T (s)	dd (°)	Q (m^3/s)	Test	H (m)	T (s)	dd (°)	Q (m^3/s)
1	/	/	/	0.002	14	0.07	1.00	20	0.005
2	/	/	/	0.0035	15	0.04	0.78	0	0.005
3	/	/	/	0.0045	16	0.05	0.90	0	0.005
4	/	/	/	0.0050	17	0.06	0.96	0	0.005
5	0.03	0.67	0	/	18	0.04	0.78	20	0.005
6	0.05	0.90	0	/	19	0.05	0.90	20	0.005
7	0.06	0.96	0	/	20	0.06	0.96	20	0.005
8	0.07	1.00	0	/	21	0.07	1.00	0	0.0035
9	0.07	1.00	0	0.002	22	0.07	1.00	0	0.0040
10	0.03	0.67	0	0.005	23	0.07	1.00	0	0.0045
11	0.07	1.00	0	0.005	24	0.07	1.00	20	0.0035
12	0.07	1.00	20	0.002	25	0.07	1.00	20	0.0040
13	0.03	0.67	20	0.005	26	0.07	1.00	20	0.0045

3. RESULTS

Measurements of beach profiles and bathymetric profiles were made. Profiles were distributed across the beach in 13 adjacent sections: one on the center-line (section A) and the others with a distance from river mouth equal to 0.27 m and from the center-line equal to 0.05 m, 0.10 m, 0.15 m, 0.20 m, 0.30 m and 0.40 m (sections B'-C'-D'-E'-F'-G') also for sections B-C-D-E-F-G (Figure 1).

All measurements were made at the end of each test for the following conditions:

- current alone
- wave alone
- combined wave-current flows

The initial profile (i0=0.05) has been re-established before at the running each test.

Figure 3 compares the beach profile along the centerline due to the current alone and the initial profile for test 4. The comparison highlights an evident beach erosion area near river mouth and a beach accretion area located at higher depth.

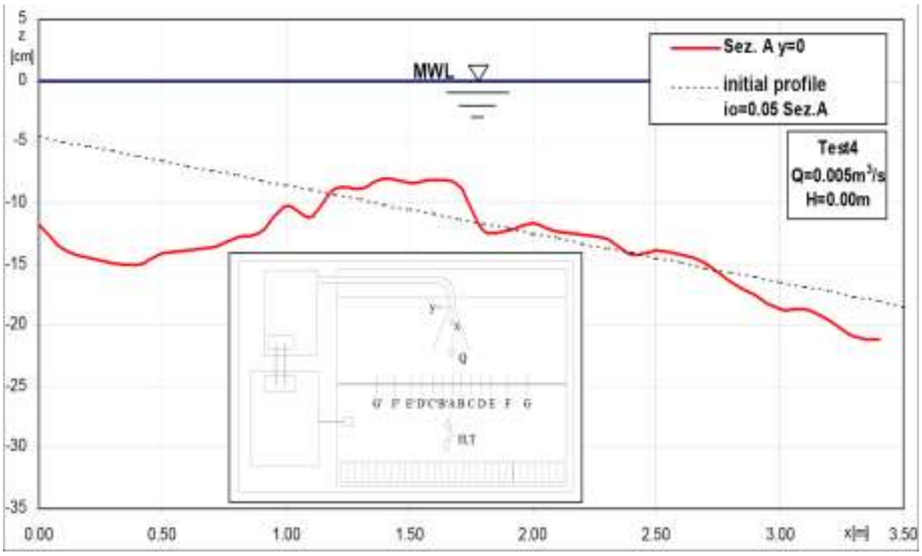

Figure 3. Beach profiles (Section A-case a-test4).

The beach profile along section A in the presence of wave alone has been compared to initial profile for test 5 (Figure 4) and the beach erosion area is less pronounced than in the current alone case.

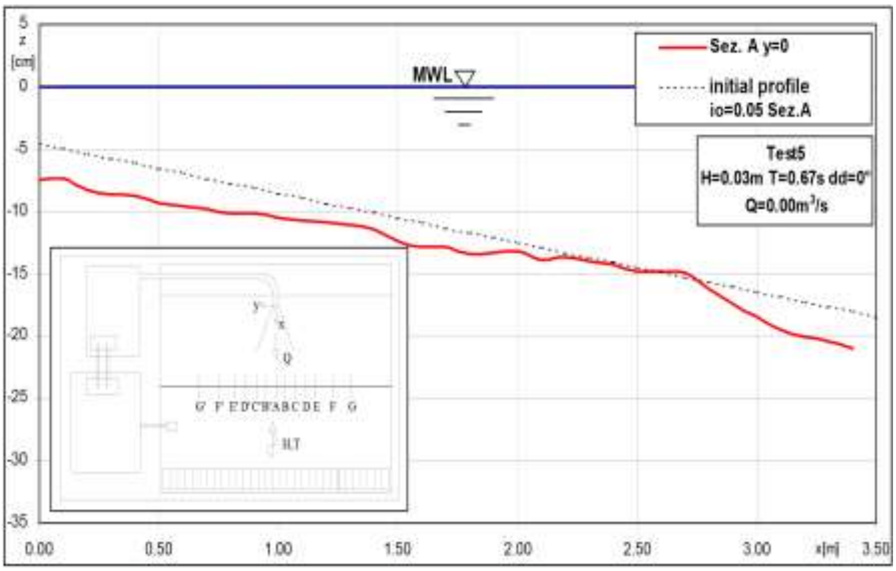

Figure 4. Beach profiles (Section A-case b-test5).

In Figures 5 ÷ 7 for tests 9, 10 and 11, the beach profiles and the bathymetric profiles due to combined wave-current flows, the initial profile and the initial modelling profile are shown. For high discharge and low wave height beach is eroded near river mouth, and an accretion area is detected at high depth (Figure 5). High wave heights combined with low discharges reduces both beach erosion and accretion (Figure 6). For both high discharge and wave height values beach erosion area is more evident while beach accretion area is not found (Figure 7).

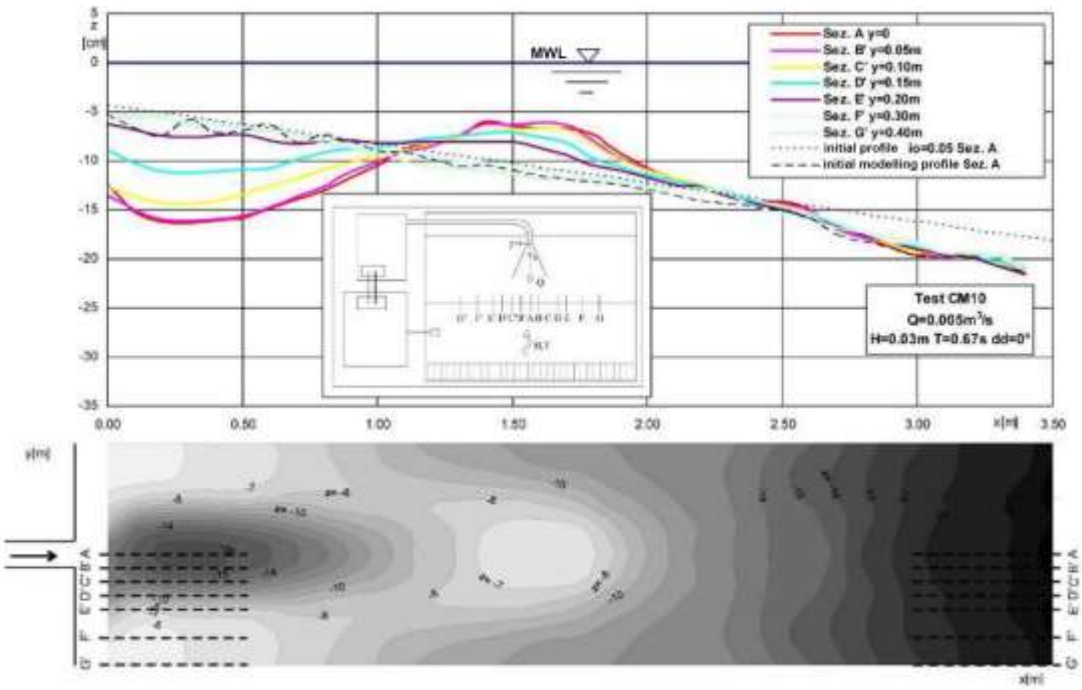

Figure 5. Beach profiles and bathymetric profiles (case c - test10).

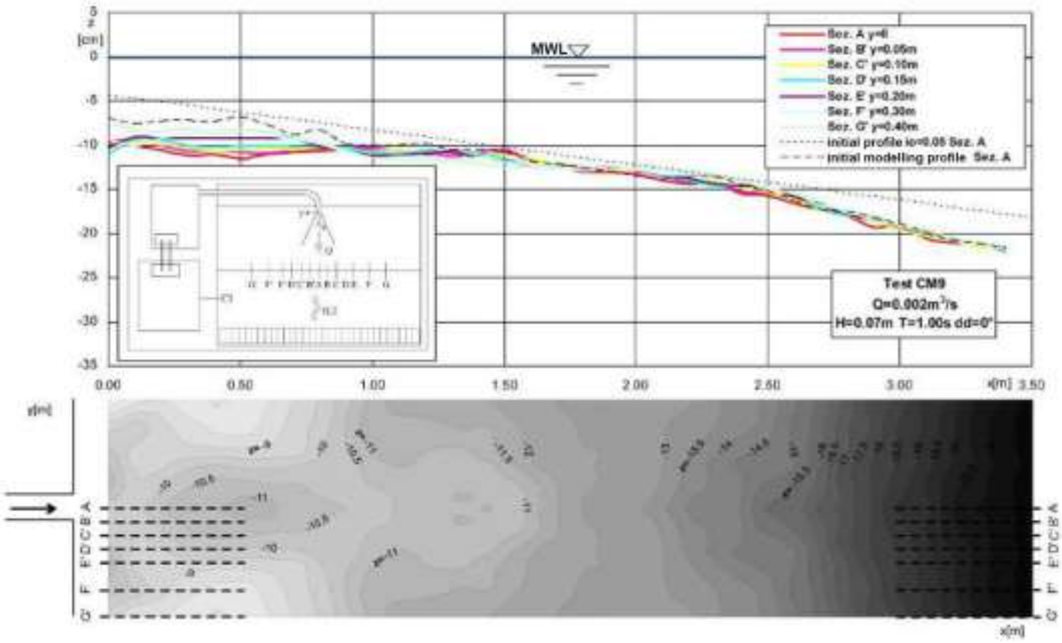

Figure 6. Beach profiles and bathymetric profiles (case c – test9).

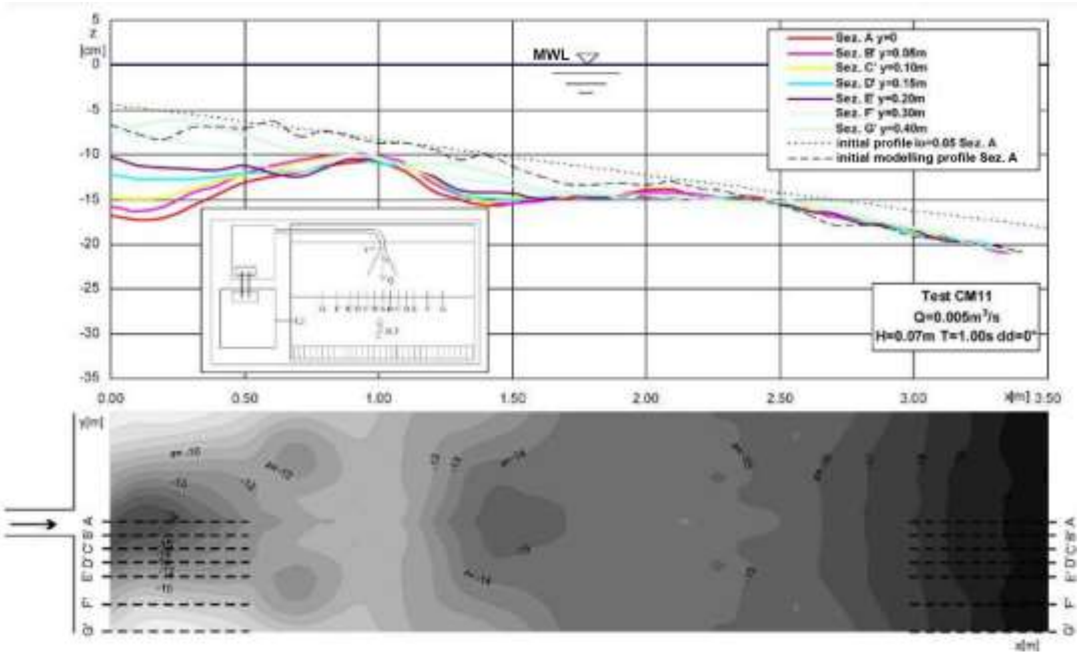

Figure 7. Beach profiles and bathymetric profiles (case c – test11).

4. DISCUSSION AND GOVERNING PARAMETERS

4.1. Beach Erosion Area Position and Depth

The results showed that the effect of the current-wave interaction increase the beach erosion close to the river mouth more than the beach accretion, especially for large discharges and low wave heights. The following dimensional parameters are introduced to analyse the beach erosion area:

- δ^{-}_{max} represents the maximum erosion depth in the beach area respect to initial profile ($i_0 = 0.05$).
- h_0 represents the water depth at inflow channel

- l^{-}_{max} represents the distance along the x-axis from river mouth where δ^{-}_{max} occurs
- S_Q represents the momentum due to the current alone evaluated at δ^{-}_{max} location
- S_H represents the momentum due to the wave alone evaluated at δ^{-}_{max} location
- S_{h0} represents the momentum due to the current alone in the steady flow condition

These parameters are shown in Figure 8.

In particular, the parameters δ^{-}_{max}/h_0 and l^{-}_{max}/h_0 have been related to the difference $S = S_Q-S_H$ respect to S_{h0} in order to highlight which is predominant forcing in each test. The momentum due to current, $S_Q = \rho V^2 h$, has been calculated using as current velocity, V, the mean value of the measurements at four points in the vertical direction at δ^{-}_{max} depth with a distance respectively of 0.035 m and from 0.025 m from sand bottom and still water level. Therefore, S_Q has been evaluated taking into account only dynamic momentum without hydrostatic term. The parameter S_{h0} has been calculated as $S_{h0} = gh_0^2/2$ where h_0 is equal to 0.108 m. Hydraulic stress, S_H, is calculated by Longuet-Higgins's formula [19] $S_H = E\,(2kh/senh2kh + 1/2)$ taking in-to account only the momentum flux rate estimating wave height, H, at δ^{-}_{max} depth.

In Figure 9 δ^{-}_{max}/h_0 is plotted against S/S_{h0} for tests 1-2-3-4 (case a), for tests 5-6-7-8 (case b) and for tests from 9 to 26 (case c).

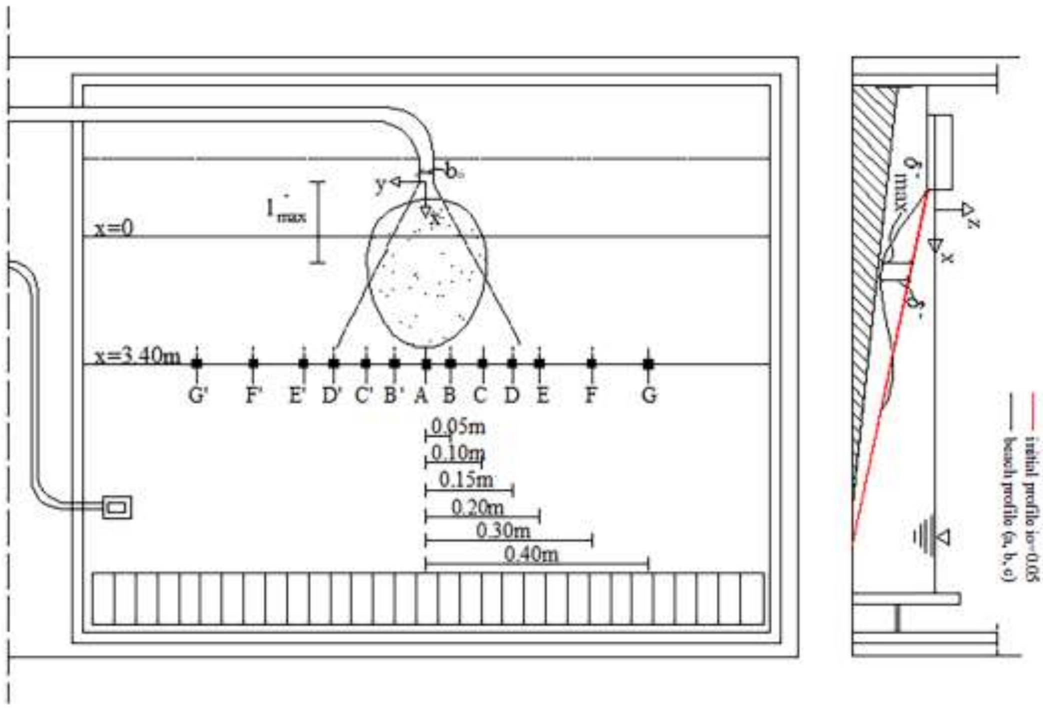

Figure 8. Beach profiles and bathymetric profiles parameters

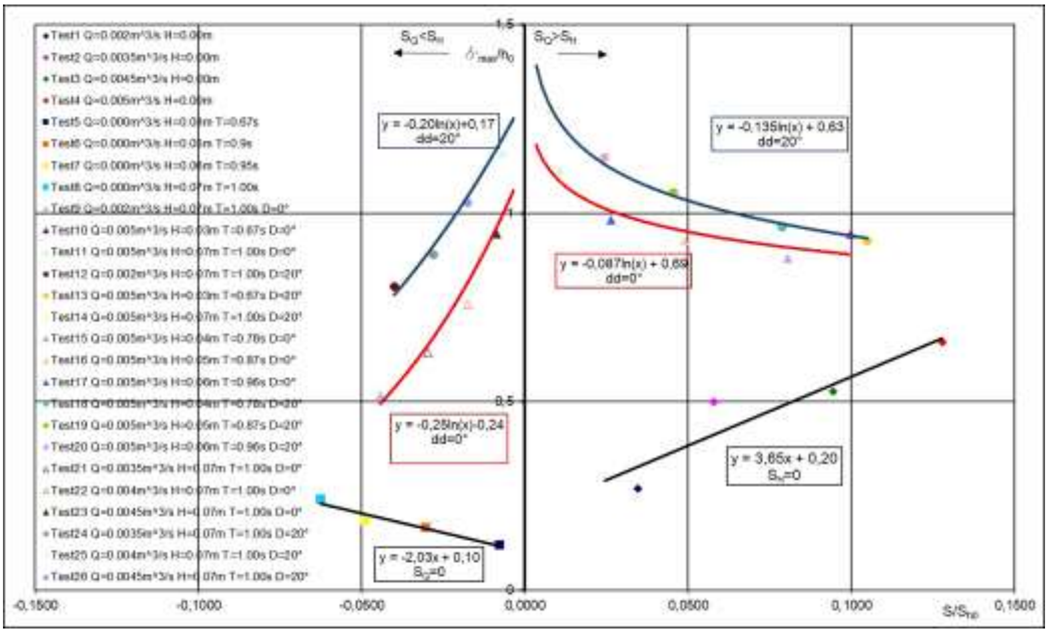

Figure 9. Parameter d-max/h0 against S/Sh0.

It is possible to underline that in presence of current alone (case a), δ^{-}_{max} maximum depth value increases with S increasing up to a maximum value δ^{-}_{max}/h_0 of 0.66 for $S/S_{h0} \cong 0.13$ (test4). In presence of wave alone (case b), δ^{-}_{max} values are smaller than for case a, increasing with S up to a maximum value of 0.24 m for $S/S_{h0} \cong 0.06$ (test8).

In presence of combined wave-current flows, for S > 0, δ^{-}_{max} values are greater than for case a, and in-crease as S decreasing for dd = 0 and dd = 20°. Moreover, for $S_Q >> S_H$ (test10 and test13), maximum depth values are not significantly affected by wave direction and values are almost equal. For S/S_{h0} approaching 0, δ^{-}_{max}/h_0 attains the highest value of 1.27 for dd = 20° (test14). For $S/S_{h0} < 0$, δ^{-}_{max} values decrease with S increasing and are higher than for case b for both wave directions. In particular, for dd = 20°, δ^{-}_{max} values are higher than for dd = 0° with a maximum value of about 1.16 for S/S_{h0} = 0.007 (test26). With the aim of providing a formula for prediction of maximum depth values of beach erosion area, δ^{-}_{max}, the best-fit equation of experimental results is shown in Figure 9. Equations 1 ÷ 6 give δ^{-}_{max}/h_0 as a function of S/S_{h0} for all the considered conditions:

$$\frac{\delta^{-}_{\max}}{h_0} = 3.65\frac{S}{S_{h_0}} + 0.20 \qquad \text{(case a - } S_H = 0\text{)} \qquad (1)$$

$$\frac{\delta^{-}_{\max}}{h_0} = -2.03\frac{S}{S_{h_0}} + 0.10 \qquad \text{(case b - } S_Q = 0\text{)} \qquad (2)$$

$$\frac{\delta^{-}_{\max}}{h_0} = -0.087\ln\left(\frac{S}{S_{h_0}}\right) + 0.69 \qquad \text{(case c - dd = 0°-} S > 0\text{)} \qquad (3)$$

$$\frac{\delta^{-}_{\max}}{h_0} = 0.135\ln\left(\frac{S}{S_{h_0}}\right) + 0.63 \qquad \text{(case c – dd = 20° - } S > 0\text{)} \qquad (4)$$

$$\frac{\delta^{-}_{\max}}{h_0} = -0.25\ln\left(\frac{S}{S_{h_0}}\right) - 0.24 \qquad \text{(case c – dd = 0° - } S < 0\text{)} \qquad (5)$$

$$\frac{\delta^{-}_{\max}}{h_0} = -0.20\ln(\frac{S}{S_{h_0}}) + 0.17 \qquad \text{(case c – dd = 20° - } S < 0) \qquad (6)$$

The l^{-}_{max}/h_0 parameter against S/S_{h0} are shown in Figure 10 for all tests. For case a, δ^{-}_{max} occurs near the river mouth at $l^{-}_{max}/h_0 \cong 4.35$ for $S/S_{h0} \cong 0.03$ (test1) and at $l^{-}_{max}/h_0 \cong 7.13$ for $S/S_{h0} \cong 0.13$ (test4).

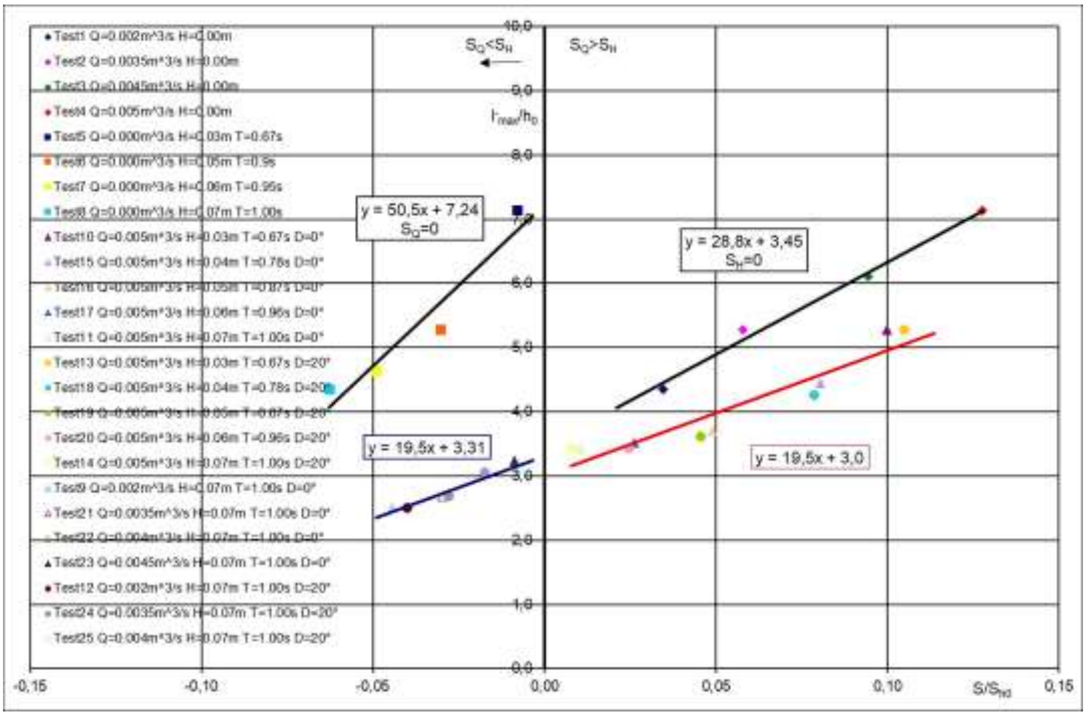

Figure 10. Parameter l-max/h0 against S/Sh0.

For case b, δ^{-}_{max} value occurs near the river mouth, $l^{-}_{max}/h_0 = 4.4$ for $S/S_{h0} \cong 0.06$ (test8) and at $l^{-}_{max}/h_0 = 7.1$ for $S/S_{h0} \cong 0.01$ (test5). In presence of combined wave –current flows, for $S > 0$, l^{-}_{max} values are smaller than in presence of current alone. In particular, l^{-}_{max} values are not influenced by wave direction and for $S_Q >> S_H$ (test10 and test13) l^{-}_{max}/h_0 is about equal to 5.3 and for S/S_{h0} approaching 0 (test11 and test14) is equal to about 3.4. For $S < 0$, l^{-}_{max} value is located closer to the river mouth than for case b with values that increase with S decreasing until reaching $l^{-}_{max}/h_0 \cong 3.7$ for $S/S_{h0} = 0.007$ (test26). Furthermore l^{-}_{max} is not influenced by wave direction. Figure 10 provides the best-fit equations of the experimental results. Equation 7 ÷ 10 relate l^{-}_{max}/h_0 to S/S_{h0} for cases a, b, c.

$$\frac{l_{\max}}{h_0} = 28.8\frac{S}{S_{h_0}} + 3.45 \qquad \text{(case a - SH = 0)} \qquad (7)$$

$$\frac{l_{\max}}{h_0} = 50.5\frac{S}{S_{h_0}} + 7.24 \qquad \text{(case b - SQ = 0)} \qquad (8)$$

$$\frac{l_{\max}}{h_0} = 19.5\frac{S}{S_{h_0}} + 3 \qquad \text{(case c - S > 0 – dd = 0° and dd = 20°)} \qquad (9)$$

$$\frac{l_{\max}}{h_0} = 19.5\frac{S}{S_{h_0}} + 3.3 \qquad \text{(case c - S < 0-dd = 0° and dd = 20°)} \qquad (10)$$

4.2. Beach Erosion Area width

The morphological changes of the beach erosion area along y-axis were analysed introducing the following parameters (Figure 8):

- δ^- represents the depth of beach erosion respect to initial profile (i_0=0.05) along the y-axis in the different measuring sections
- δ^+ represents the height of beach accretion evaluated respect to initial profile (i_0=0.05) along the y-axis in the different measuring section
- l_L is the ratio of the distance y of each measurement section from central section A respect to in-flow channel width b_0 (b_0 = 0.20 m)

In Figure 11, for example, δ^- values are plotted against l_L for test10. For high discharge and wave height values, δ^- values reduce to zero away from river mouth (x = 2.67 m). Along y-axis, δ^- follows a bump-like distribution and for l_L = 2 δ^- = 0 at x = 2.67 m and δ^- = 0.014 m at x = 0.27 m. δ^+ values also follow a bump-like distribution and δ^+ = 0 at x = 2.67 as shown in Figure 12.

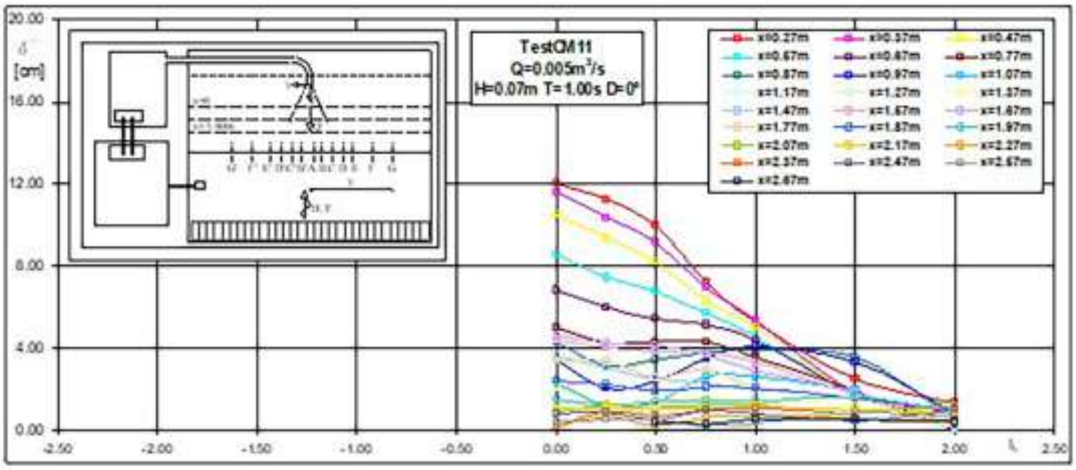

Figure 11. Parameter δ^- against l_L.

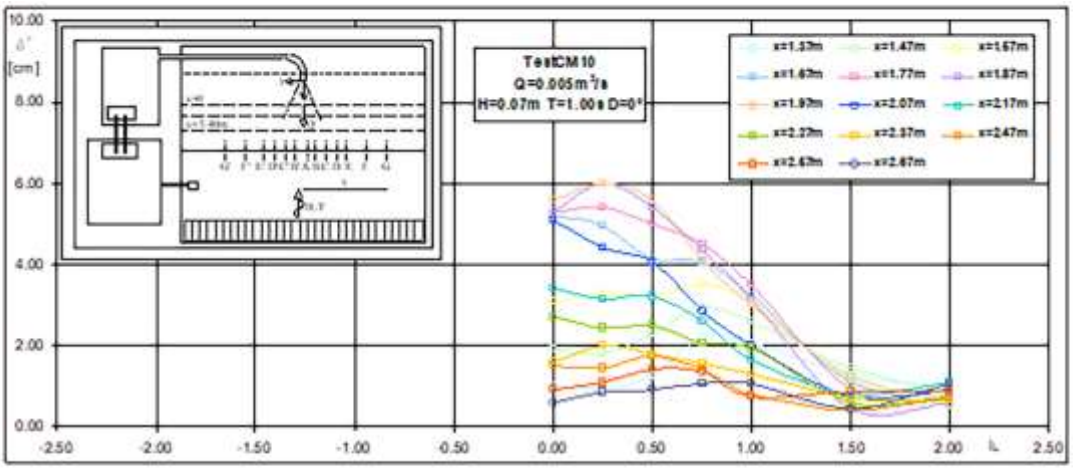

Figure 12. Parameter δ^+ against l_L.

Furthermore, from the above observations it has been defined the beach erosion area width for all tests introducing several additional parameters (Figure 8):

- S_0 is the ratio of the hydraulic stress due to wave alone, S_{H0}, to hydraulic stress due to current alone, S_{Q0}. The S_{H0} value is evaluated at wave gauges positioned on array, while S_{Q0} value is evaluated at channel outlet;
- $l^*_L = l_{L25\%}$ represents the value of l_L where δ^- depth value is equal to 25% of δ^-_{max} maximum depth value.

In Figure 13 l^*_L values are plotted against $S_0 = S_{H0} / S_{Q0}$. As it can be seen, l^*_L values are greater for dd = 0° in all experimental conditions. For instance, for $S_0 \cong 0.55$ (test9) that is $S_{H0} \cong 0.55SQ_0$, l^*_L value is equal to 4.00 and beach erosion area width, y, is equal to 4 times b_0. As So decreases to $S_0 \cong 0.02$, it is $S_{H0} \cong 0.02\ S_{Q0}$ (test10), l^*_L value is equal to 2.00 and y is equal to 2 times b_0. For dd = 20°, l^*_L values are equal to 3.20 for $S_0 = 0.55$ (test12) and equal to 1.70 for $S_0 \cong 0.02$ (test13). This means that the width of the beach erosion area, y, is greater than b_0, whatever the hydraulic stress value.

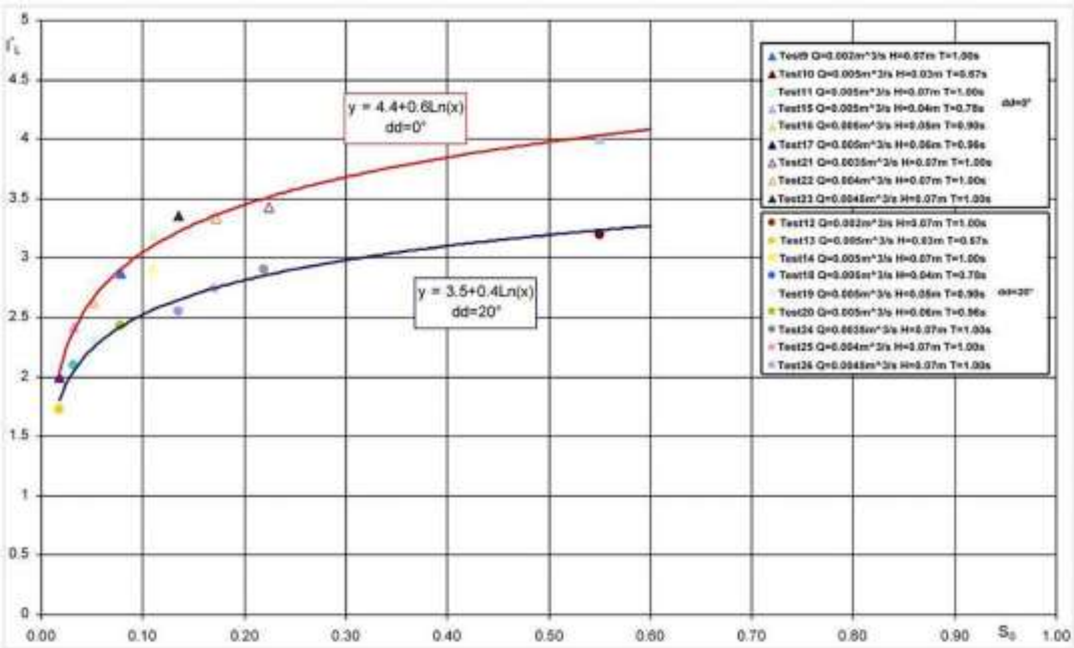

Figure 13. Parameter l^*_L against S_0 for all tests

Figure 13 reports the best-fit equation of the experimental results. Equations 11 - 12 give l^*_L values as a function of S_0 for case c.

$$l_{L*} = 4.4 + 0.6\ln(S_0)\ \text{(case c – dd = 0°)} \qquad (11)$$

$$l_{L*} = 3.5 + 0.4\ln(S_0)\ \text{(case c – dd = 20°)} \qquad (12)$$

4.2. Sediment Balance

The beach and bathymetric profiles shown highlight an evident erosion process close to the river mouth in presence of combined wave-current flow. The depth and width values of beach erosion area are greater than the width and depth values of channel inflow. This result has been highlighted also by sediment balance analysis for wave-current interaction within measurement area. The accretion and erosion volumes, W^+ and W^-, respectively, were estimated respect to the initial profile, i_0=0.05 for tests 9 ÷ 14. Furthermore, the parameter D = W^+-W^- has been introduced. Table 2 reports the values of W^+, W^- and D. The results highlight that D values are always negative. This means that the wave-current interaction has determined greater beach erosion than accretion. For dd = 0°, D increases with high discharge and high wave height (test11) and reduces to zero in presence of high discharge and low wave height (test10). Likewise, for dd = 20°, sediment balance is still negative reaching higher values for $S_H \cong S_Q$.

Table 2. Parameter W^+, W^- and D.

Test	**W^+ (m^3)**	**W^- (m^3)**	**Δ (m^3)**	**Test**	**W^+ (m^3)**	**W^- (m^3)**	**Δ (m^3)**
9	0.0034	0.0200	-0.0166	12	0.0060	0.0300	-0.0240
10	0.0197	0.0258	-0.0061	13	0.0172	0.0209	-0.0037
11	0.0026	0.0480	-0.0454	14	0.0045	0.0374	-0.0329

5. CONCLUSION

Coastal morphological processes is strongly influenced by the combined current – wave flow with an evident erosion area located in vicinity of river mouth. This study was carried out in a 3D wave basin of the Hydraulics Laboratory of the University of Campania "Luigi Vanvitelli". The experimental tests have been running with bottom sand subjected to the following conditions:

a. current alone

b. wave alone

c. combined wave –current flows

The key conclusions are as follows:

- the current alone (case a) determines more pronounced beach erosion area located near river mouth respect to in presence of wave alone (case b);
- the current-wave interaction (case c) determines, beach erosion area located near river mouth greater than in case a and b.

In particular, in the case of combined wave-current flows, wave direction influences the value of maximum depth of beach erosion, which is greater for dd = 20°. The maximum depth position of beach erosion area not depends significantly by wave direction. The parameters, d^-_{max}/h_0, and l^-_{max}/h_0, varying with S/S_{h0}, are best-fit by equation (1 ÷ 10). The tests carried out have shown also that beach erosion area width is greater for high current value and low wave height and for wave direction dd = 0°. The best-fit equation of experimental results is equation 11 ÷ 12 that give l^*_L values varying S_0. The experimental results obtained have been highlighted also by sediment balance analysis for wave-current interaction within measurement area. The erosion volumes were greater than accretion volumes that become significant for high discharge and high wave height values, for both wave propagation dd = 0° and dd = 20°. By experimental results shown it can be derived that the presence of the current causes an increase in the wave height, and therefore an increase in the wave energy near river mouth, thus determining wave breaking and consequently greater erosion process.

ACKNOWLEDGEMENTS

The authors acknowledge the financial grant program VALERE: "VAnviteLli pEr la RicErca

REFERENCES

[1] Ismail, N.M. Effect of opposing wave on the mixing of a surface horizontal jet. In Technical Report HEL27-9, Hydraulic and Coastal Engineering, Division University of California, 1981.

[2] Ismail, N.M.; Wiegel, R.L. Opposing wave effect on momentum jets spreading rate. J Waterw Port Coast, 109 (4), 465-483. 1983

[3] Koole, R.; Swan, C. Measurements of a 2-D non-buoyant jet in a wave environment. Coast. Eng. 24, pp.151-169. 1994

[4] Di Natale, M. Nonlinear hydrodymamic effects of opposing jet-current on waves. Proceedings of ISOPE, 1998.

[5] Di Natale, M.; Vicinanza, D. Experimental velocity profiles in wave-jet interaction. Proceedings of ISOPE, 2000.

[6] Skafel, M.G. Laboratory measurement of nearshore velocities and erosion of cohesive sediment (till) shorelines. Coast. Eng. 24, 343-349. 1995

[7] Seabergh, W.C.; King, Jr.D.B.; Stephens, B.E. Tidal inlet equilibrium area experiment, inlet laboratory investigation. In Technical Report, Coastal Inlet Research Program, U.S. Army Corps of Engineers, 2002.

[8] Ozolcher, I.H. An experimental study on geometric characteristics of beach erosion profiles. Ocean Eng. 35, 17-27. 2008

[9] Cáceres, I.; Grüne, J.; Van Rijn, L.; Sánchez-Arcilla, A.; Ahmari, A.; Ribberink, J. Mobile-bed tests: the sands project. Coast. Eng. 2622-2632. 2008

[10] Lee, W.D.; Mizutani, N.; Hur, D.S. Experimental analysis of wave deformation and bottom flow under wave current interaction in the river mouth. Ocean Eng. 140, 169-182. 2017

[11] Bosa, S.; Petti, M.; Lubrano, F.; Pascolo S. Morphodynamic model suitable for river flow and wave current interaction. In IOP Conference Materials Science and Engineering, 2017.

[12] Bosa, S.; Petti, M.; Lubrano, F.; Pascolo, S. Finite volume morphodynamic model useful in coastal environment. Procedia Eng. 161, 1887-1892. 2016

[13] Pascolo, S.; Petti, M.; Bosa, S. Wave-current interaction: a 2DH model for turbolent jet and bottom-friction Dissipation. Water, 10 (392), 2018. DOI: 10.3390/w10040392.

[14] Frigaard, P.; Brorsen, M. A time domain method for separating incident and reflected irregular waves. Coast. Eng. 24. 1995

[15] Di Natale, M.; Eramo, C.; Vicinanza, D. Realizzazione di un impianto sperimentale per lo studio degli effetti della subsidenza sulla dinamica di una spiaggia emersa. Proceedings of XXIX Convegno di Idraulica e Costruzioni Idrauliche, Trento, Italy, 761–768. 2004

[16] Di Natale, M., Eramo, C. Vicinanza, D. Experimental investigation on beach morphodynamics in presence of subsidence. J. Coast. Res. 222-231. 2008

[17] Eramo, C. Modellazione fisica dei processi di erosione costiera in presenza di fenomeni di subsidenza. Ph.D. Thesis, Università degli Studi Di Napoli “Federico II”, Napoli, Febbraio 2005.

[18] U.S. Army Corps of Engineers, Shore Protection Manual, Coastal Engineering Research Centre (CERC), 1994.

[19] Longuet-Higgins, M.S. Longshore currents generated by obliquely incident waves. J Geophys Res,75 (33), 6778-6801. 1970

[20] Minutolo V., Palladino S., Ferla P., Zona R., Esposito L. and Di Natale M. Non-Linear strain analysis of coupled sub-marine pipelines during the launch phase. International Journal of Civil Engineering and Technology. pp. 53-63. 2020.

[21] Angelina A. Kolomeytseva, A Review Current Trends in the Development of Renewable Sources of Energy, International Journal of Mechanical Engineering and Technology, 9(10), pp. 1593–1602. 2018

[22] Kiran Raj Bukkarapu, Y. Jyothi, L. S. Raju, G. Chitti Babu and Karthik Narayanan, A Review on Current Trends in Water in Oil Emulsions, International Journal of Mechanical Engineering and Technology, 8(4), pp. 359-371, 2017

[23] B. Lakshmi.R, A Single Rating Inductor Multilevel Current Source Inverter with PWM Strategies and Fuzzy Logic Control, International Journal of Electrical Engineering and Technology, 8(4), pp. 359-371, 2017